ISBN: 978-3-95450-184-7 doi:10.18429/JACoW-IPAC2018-WEPMK005

PRELIMINARY RESULTS FROM VALIDATION MEASUREMENTS OF THE LONGITUDINAL POWER DEPOSITION MODEL FOR THE LHC INJECTION KICKER MAGNET*

V. Vlachodimitropoulos†, M.J. Barnes, A. Chmielinska,
CERN, Geneva, Switzerland

Abstract

During Run 1 of the LHC, one of the injection kicker magnets (MKIs) exhibited an excessively high ferrite temperature, caused by coupling of the high intensity beam to the real impedance of the magnet. Beam-screen upgrades, implemented during Long Shutdown 1 (LS1), have been very effective in reducing beam coupling impedance and since then the MKIs have not limited LHC's availability. However, temperature measurements during operation have shown that one end of the MKI's ferrite yoke is consistently hotter than the other. Detailed simulation models and data post-processing algorithms have been developed to understand and mitigate the observed behaviour. In the present paper, the model used to obtain the power loss distribution along the magnet is presented. The model is subsequently applied to two MKI design configurations under study: (i) the one currently in operation and (ii) an upgraded magnet that was installed in the LHC tunnel during the Year End Technical Stop (YETS) 2017/18. In order to validate the expected behaviour a novel measurement technique was developed, applied in both configurations and compared to predictions. The results obtained are reported and conclusions regarding the effectiveness of the design are drawn.

INTRODUCTION

Temperatures of the MKI ferrite yokes are critical to LHC's performance and total luminosity production. If the ferrite Curie temperature is exceeded, long turnaround times are required to cool down the yoke before beam can be injected into the LHC [1]. In order to monitor the temperatures, four PT100 temperature probes, two per magnet end [2], are installed in each of the four MKI kicker modules at both injection points. Operational experience during Run 2 has shown that the upstream (beam entrance) end of the magnet is consistently hotter than the downstream end [3].

The observed longitudinal temperature difference has been attributed to the longitudinal asymmetry of the MKI beam screen design. A set of 24 NiCr conducting wires placed at the inner wall of a slotted alumina tube provide a conducting path for the beam image currents thus shielding the ferrite yokes (CMD5005 [4] or 8C11 [5]) from the electromagnetic (e/m) field of the circulating beam. To avoid excessive eddy currents, which would impair the rise time of the pulsed field, the screen conductors are not grounded at both ends of the magnet. Instead, they are directly connected to the local ground at the downstream end and capacitively coupled to a grounded metallic cylinder at the upstream end. The capacitively coupled end acts as an open-ended, $\lambda/2$-coaxial resonator that extracts power from the beam at multiples of its fundamental frequency and subsequently couples it to the tank, thus affecting the upstream end parts of the magnet more. Finally, a set of nine ferrite rings, Ferroxcube [5] ferrite types 4B3 and 4M2 used alternately, are placed at each end of the alumina tube aiming to damp low frequency, $\lambda/4$-modes that could develop along the screen conductors. The current (post-LS1) MKI beam screen is shown in Fig. 1.

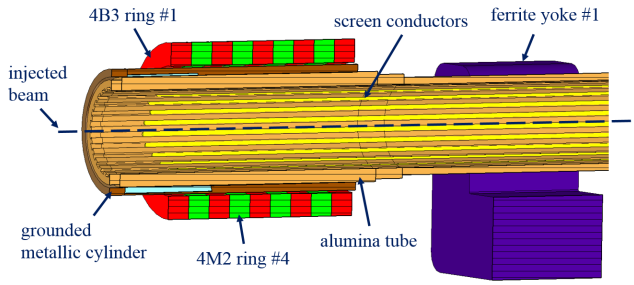

Figure 1: Simplified schematic of the post-LS1 beam screen.

THE MODEL

To quantify the observed behaviour and estimate the dissipated e/m power, a detailed model was developed using CST Particle Studio [6] and simple data post-processing. The goal of the model is to provide the power loss distribution along the length of the magnet P_i, i.e. the dissipated power in the i-th ferrite component (ring or yoke).

For the LHC type beams with a 25-ns bunch spacing filling scheme, the power of the beam is mainly concentrated at multiples of 40 MHz. Therefore P_i can be approximated as:

$$P_i \approx \sum_{n=1}^{+\infty} P_i(\omega_n) = P_L \sum_{n=1}^{+\infty} \alpha(\omega_n)\hat{p}_i(\omega_n), \qquad (1)$$

where $P_i(\omega_n)$ is the power dissipated at the i-th solid at frequency $\omega_n = n \times 40\,\text{MHz}$, P_L is the total power dissipated in the magnet, $\alpha_n = P(\omega_n)/P_L$ is the power loss at frequency ω_n normalised to the total power P_L, and $\hat{p}_i(\omega_n)$ is the normalised power deposition distribution at frequency ω_n subject to the condition $\sum_{i=1}^{S} \hat{p}_i(\omega_n) = 1$, where S is the total number of solids in which e/m power is dissipated.

* Work supported by the HL-LHC project.
† vasileios.vlachodimitropoulos@cern.ch

ISBN: 978-3-95450-184-7 doi:10.18429/JACoW-IPAC2018-WEPMK005

The first two terms on the right hand side (RHS) of (1) can be directly obtained from the following formula for RF losses:

$$P_L = I_b^2 \sum_{p=1}^{\infty} |\hat{\lambda}(p\,\omega_0)|^2 \Re\{Z_L(p\,\omega_0)\}\,, \qquad (2)$$

where I_b is the average beam current, ω_0 the revolution frequency in the machine, $\hat{\lambda}$ the Fourier transform of the normalised beam current and Z_L the longitudinal impedance of the device under consideration. The last term is obtained from CST simulations by placing power loss field monitors at the required frequencies and subsequently normalising to the total losses at every frequency, i.e.

$$\hat{p}_i(\omega_n) \equiv \frac{P_i^{\mathrm{CST}}(\omega_n)}{\sum_{i=1}^{S} P_i^{\mathrm{CST}}(\omega_n)}\,, \qquad (3)$$

where $P_i^{\mathrm{CST}}(\omega_n)$ is the CST estimated power dissipation in the i-th solid at frequency ω_n.

Model Predictions

The model was used to estimate the power loss longitudinal distribution in two MKIs featuring different beam screen designs; one design has been in operation since the end of LS1 and one that was implemented in an upgraded magnet installed in the LHC tunnel during the YETS 2017/18. The main, thermally related, modification in the latter was the reduced overlap length of the capacitive coupling at the upstream end of the magnet in order to reduce the generated the RF losses. A detailed description of the new magnet can be found in [7, 8].

Power loss monitors, at multiples of 40 MHz, were used at frequencies up to 1.2 GHz. At this frequency the RF losses have sufficiently reduced and more monitors would not noticeably improve the result. Previously, less field monitors were used, mainly around the resonant impedance modes, where most of the power was expected to be lost. Although more demanding from a data storage point of view, the current approach was eventually adopted to improve the accuracy of the predictions.

A comparison of the power deposition, for the two beam screen designs, in the nine upstream ferrite rings and the first six yokes is shown in Fig. 2, where the redistribution of the power loss is evident. In the post-LS1 design only 9 W, or 18% of the total power deposition (51 W), is dissipated in the ferrite rings. However, in the upgraded design the amount increases to 33 W, or 89% of the reduced total power loss (37 W). Consequently, predictions show that the dissipated power in the first yoke is reduced from 10 W to 0.45 W, i.e. an overall reduction of more than 95%.

MODEL VALIDATION

The Setup

To validate the predictions, a simple measurement setup was constructed based on ideas from standard impedance

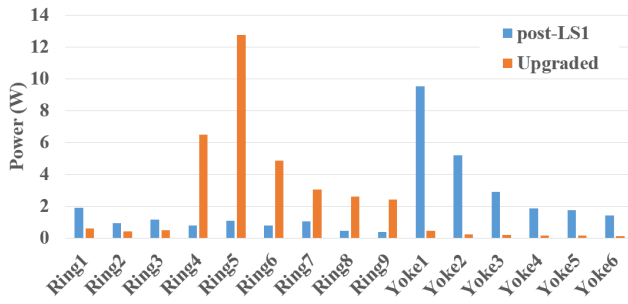

Figure 2: Distribution of power dissipation along two MKIs with different beam screen designs.

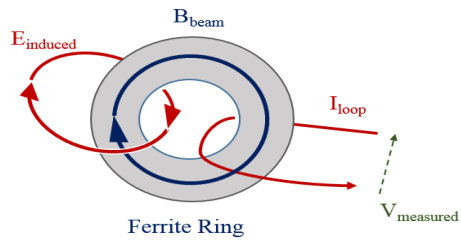

Figure 3: Schematic of the magnetic field detection technique.

measurement techniques [9]. The goal of the measurement was to compare the magnetic (B) field that couples to the different ferrites of the MKI, as magnetic losses are the main mechanism of power dissipation in the ferrites. The technique is based on the observation from simulations that the e/m modes which couple to the ferrite rings and yokes are nearly TEM, with the B-field directed azimuthally (see Fig. 3). Therefore, single-loop probes were placed around two of the ferrite rings (#1 and #5), as shown in Fig. 4, and at the first ferrite yoke, to measure the voltage that is induced by the changing magnetic field.

Due to mechanical constraints, a probe was not placed around a leg of the U-shaped yoke. Instead, Kapton tape was used to fix it on the yoke's outer side – this results in weaker coupling to the magnetic field and hence a smaller measured signal. Although the probes were not optimally located, conclusions based on a qualitative comparison are still possible to draw.

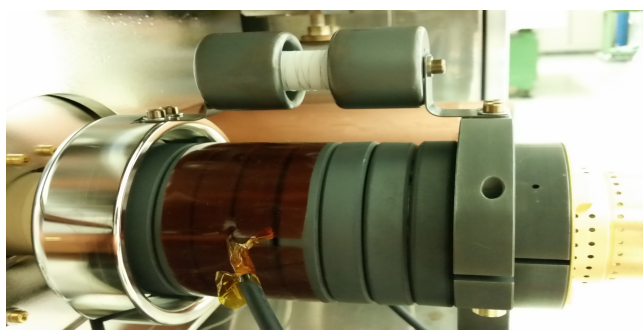

Figure 4: Probe placed at the fifth ferrite ring (incoming beam from the right).

ISBN: 978-3-95450-184-7 doi:10.18429/JACoW-IPAC2018-WEPMK005

To excite the magnet with the TEM field of the relativistic circulating beam, a copper wire of 0.5 mm diameter is stretched along the aperture of an MKI magnet. The wire together with the beam screen conductors form a coaxial line whose fundamental TEM mode is excited at the upstream end via port 1 of a Vector Network Analyzer (VNA). Low inductance carbon resistors of ~220 Ω were mounted at each end of the magnet to match the impedance of the ~270 Ω coaxial line to the 50 Ω VNA cables. Since only a 2-port VNA was available for the measurement, the downstream end of coaxial line was terminated in a 50 Ω load, while port 2 of the VNA was connected to the probes; the transmission parameter S_{21} was recorded.

Results

In Fig. 5 the measured signal at the three probes is presented for each of the two designs under study. In addition, for each design, the real part of the simulated longitudinal impedance, whose coupling to the beam spectrum gives rise to RF losses, is plotted on a separate axis. In agreement with expectations, the measured signal at the probes is stronger at the resonant frequencies of the impedance mode. This verifies the prediction that in the upgraded design losses will occur at higher frequencies, where the beam power spectrum is reduced. Therefore lower overall RF losses are expected.

Of particular interest is a comparison of the measured signal at the probe next to the first yoke. As shown in Fig. 6, a reduction of more than 30 dB is observed for frequencies below 1 GHz in the upgraded design compared to the one for post-LS1. This result is in good qualitative agreement to the predictions for the power loss distribution, see Fig. 2, and increase confidence in the effectiveness of the modified beam screen.

Nonetheless not all results verify the predictions. In particular, for the upgraded design, although the signals measured at ring 1 and yoke 1 are comparable, in agreement with predictions for the corresponding losses, they appear slightly stronger than the one measured at ring 5. The latter was expected to be significantly stronger than the former two, as losses in ring 5 are predicted to be much higher than in the other two ferrites. Studies to understand these discrepancies are ongoing.

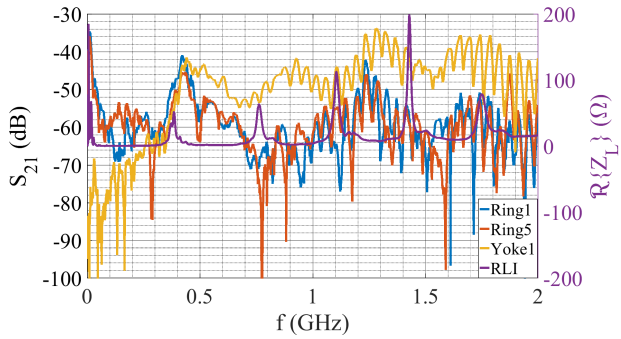

(a)

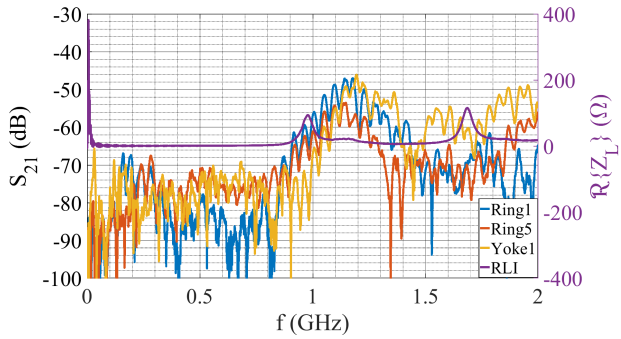

(b)

Figure 5: Comparison of the measured signals for each design: (a) post-LS1 and (b) Upgraded.

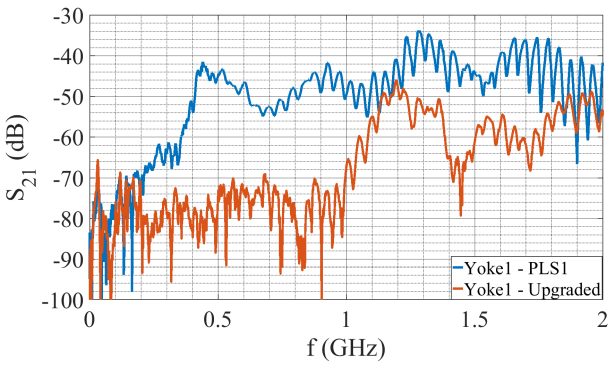

Figure 6: Comparison of the measured signal at the probe next to yoke 1.

SUMMARY AND FUTURE WORK

In the present work a model to obtain the power loss distribution in structures with various lossy components was presented and applied to two MKIs featuring different beam screen designs. To validate the predictions, a novel measurement technique was developed and implemented. Results of the measurements were reported showing partial qualitative agreement between the model and the measurements. Nonetheless, discrepancies between the model predictions and the measurement results were also observed.

Studies are ongoing to further validate the model and improve the measurement technique. Understanding the source and mitigating the observed discrepancies between predictions and measurements is necessary to properly validate the theoretical model and thus comprehend the power loss distribution along the MKI. Eventually, this would allow to accurately estimate the magnet's thermal behaviour.

ACKNOWLEDGEMENTS

The authors would like to thank G. Bellotto, S. Bouleghlimat, P. Goll and Y. Sillanoli for preparing the measurement setup.

ISBN: 978-3-95450-184-7 doi:10.18429/JACoW-IPAC2018-WEPMK005

REFERENCES

[1] M.J. Barnes *et al*., “Beam induced ferrite heating of the LHC injection kickers and proposals for improved cooling”, in *Proc. IPAC’13*, Shanghai, China, May 2013, paper MOPWA031, pp. 732-734.

[2] L. Vega Cid, M.J. Barnes, V. Vlachodimitropoulos, W. Weterings, and A. Abánades. "Thermal analysis of the LHC injection kicker magnets", in *Proc. IPAC’17*, Copenhagen, Denmark, May 2017.

[3] V. Vlachodimitropoulos *et al*., "Hardware limitations at injection", in *Proc. 8th LHC Operations Workshop*, Evian, France, December 2017.

[4] http://www.cmi-ferrite.com

[5] http://www.ferroxcube.com

[6] http://www.cst.com

[7] V. Vlachodimitropoulos, M.J. Barnes, L. Ducimetière, L. Vega Cid, W. Weterings, "Longitudinal impedance analysis of an upgraded LHC injection kicker magnet", presented at IPAC’18, Vancouver, Canada, May 2018, paper WEPMK002.

[8] M.J. Barnes *et al*., "An upgraded LHC injection kicker magnet", presented at IPAC’18, Vancouver, Canada, May 2018, paper WEPMK003.

[9] T. Kroyer, F. Caspers, and E. Gaxiola, "Longitudinal and transverse wire measurements for the evaluation of impedance reduction measures on the MKE extraction kickers", CERN, Geneva, Switzerland, CERN Technical Note AB-Note-2007-028.